

**KfK 3568**  
**August 1983**

# **Out-of-pile Bundle Temperature Escalation under Severe Fuel Damage Conditions**

**S. Hagen, S. O. Peck**  
**Hauptabteilung Ingenieurtechnik**  
**Projekt Nukleare Sicherheit**

**Kernforschungszentrum Karlsruhe**



KERNFORSCHUNGSZENTRUM KARLSRUHE  
HAUPTABTEILUNG INGENIEURTECHNIK  
PROJEKT NUKLEARE SICHERHEIT

Kfk 3568

**Out-of-pile Bundle Temperature Escalation  
under Severe Fuel Damage Conditions.**

S. Hagen, S.O. Peck<sup>+</sup>)

<sup>+</sup>) USNRC Delegate to Kernforschungszentrum Karlsruhe  
from EG&G, Idaho Falls, Idaho.

KERNFORSCHUNGSZENTRUM KARLSRUHE GMBH, KARLSRUHE

Als Manuskript vervielfältigt  
Für diesen Bericht behalten wir uns alle Rechte vor

Kernforschungszentrum Karlsruhe GmbH  
ISSN 0303-4003

## Out-of-Pile Bündelexperimente zur Temperatureskalation bei schweren Kernschäden

---

### Kurzfassung

Dieser Bericht gibt einen Überblick über die Durchführung und die Ergebnisse des Bündeltests ESBU-1. Der Versuch diente der Untersuchung der Temperatureskalation in Bündelgeometrie und der damit verbundenen Schadensmechanismen. Die Eskalation wird durch die exotherme Zirkon-Wasserdampf-Reaktion hervorgerufen. Es wurde ein 3x3 Bündel umgeben von einem Zirkaloy-Dampfführungskasten und 6 mm Keramikfaserisolation untersucht.

Die maximale Oberflächentemperatur des Zirkaloystabs erreichte ca. 2250°C. Die Begrenzung der Eskalationstemperatur wurde bei dem hier vorliegenden Versuch im wesentlichen durch Abfließen des geschmolzenen Zirkaloy aus dem Reaktionsbereich hervorgerufen.

Die Nachuntersuchung ergab folgendes Ergebnis: In der Anfangsphase bildet sich eine dünne Oxidschicht, diese wird durch das ablaufende geschmolzene Zirkaloy des inneren Hüllrohrbereichs mit in den unteren Bereich gespült und aufgelöst. Die ablaufende Schmelze löste nur die Oberfläche der Pellets in knapp 0,5 mm Stärke. Das Schmelzgut erstarrte im unteren Bereich des Bündels zu einem zusammenhängenden Klumpen. Beim Abkühlen zerbröselte ein merklicher Teil der Pellets und bildete einen Haufen aus puderförmigen Teilchen auf dem Schmelzklumpen.

Untersuchungen mit dem Metallmikroskop und der Mikrosonde haben gezeigt, daß die Schmelze sowohl UO<sub>2</sub> gelöst hat als auch teilweise mit dem entstandenen ZrO<sub>2</sub> in Wechselwirkung tritt. Durch Wechselwirkung mit dem Dampf wird die Schmelze selber bis zur Bildung eines (U,Zr)O<sub>2</sub> Mischoxids aufoxidiert.

## Abstract

This report provides an overview of the test conduct, results, and posttest appearance of bundle test ESBU-1. The purpose of the test was to investigate fuel rod temperature escalation due to the exothermal zircaloy/steam reaction in a bundle geometry. The 3x3 bundle was surrounded by a zircaloy shroud and 6 mm of fiber ceramic insulation.

The center rod escalated to a maximum of 2250°C. Runoff of the melt apparently limited the escalation. Posttest visual examination of the bundle showed that cladding from every rod had melted, liquefied some fuel, flowed down the rod, and frozen in a solid mass that substantially blocked all flow channels. A large amount of powdery rubble, probably fuel that fractured during cooldown, was found on top of the blockage. Metallographic, EMP, and SEM examinations showed that the melt had dissolved both fuel and oxidized cladding, and had itself been oxidized by steam.

Contents

	Page
1. Introduction	3
2. Test Conduct	4
3. Test Results	4
3.1 Bundle Temperatures	4
3.2 Posttest Appearance	5
3.3 Posttest Examination	6
3.3.1 Appearance of the Bundle Blockage	6
3.3.2 Dissolution of UO <sub>2</sub> by the Melt	7
3.3.3 Phases in the Refrozen Melt	8
3.3.4 Dissolution of Oxidized Cladding by the Melt	8
3.3.5 Oxidation of Cladding and Melt by Steam	9
4. Summary	10
5. Acknowledgement	10
6. References	11
7. List of Figures	12



## 1. Introduction

As part of the German Nuclear Safety Project, out-of-pile experiments have been performed at the Kernforschungszentrum Karlsruhe investigating the behavior of fuel rod simulators under severe fuel damage conditions. These experiments will provide data on the mechanisms damaging PWR fuel rods at temperatures up to 2200°C.

Earlier experiments have shown that the behavior of fuel rods in this temperature range is strongly dependent on the degree of cladding oxidation. The oxidation depends in part on the temperature rise rate. The rise rate itself may be influenced by the exothermic oxidation process. As long as the heat produced by oxidation exceeds the heat losses, the temperature will escalate. Therefore, oxidation-induced temperature escalation may play an important role in determining fuel behavior. To investigate temperature escalation and processes leading to a turnaround of the escalation, a series of single rod and bundle experiments have been performed as part of the Severe Fuel Damage Program. This paper discusses the results of the nine-rod bundle experiment ESBU-1 /1/.

The results of the single rod experiments /2,3,4/ have shown that, independent of the initial heatup rate (0.3-4°C/s), a temperature escalation was observed in every test. The maximum temperature rise rate was about 6°C/s in each test. Maximum cladding surface temperatures never exceeded 2200°C. The temperature at which the escalation began increased with decreasing initial heatup rate. Posttest examination showed that runoff of molten zircaloy limited the escalation for fast initial heatup rates, and a protective oxide layer at slow initial heatup rates.

## 2. Test Conduct

The bundle was composed of a 3x3 array of fuel rod simulators surrounded by a zircaloy shroud which was insulated with a 6-mm ZrO<sub>2</sub> fiber ceramic wrap as shown in Figure 1. The fuel rod simulator comprised a 6.0-mm tungsten heater, UO<sub>2</sub> annular pellets, and 10.75-mm zircaloy cladding over a 400-mm heated length. A steam flow of 0.093 g/s per rod was inlet to the bundle. Power was applied sufficient to cause about a 2°C/s heatup rate until the temperature escalation due to zircaloy oxidation heating raised the heatup rate to about 6°C/s (Figure 2).

Temperatures were measured by two color pyrometers on three surfaces 145 mm from the bundle top end: (a) shroud outer surface, (b) cladding surface of a side rod, and (c) cladding surface of the center rod (made possible by removing a portion of one of the side rods at the pyrometer elevation). Ni-CrNi thermocouples with Inconel sheaths were used to measure cladding surface temperatures at the bundle top and bottom, the steam exit temperature, and shroud and insulation temperatures at the bundle top, bottom, and pyrometer elevation.

## 3. Test Results

### 3.1 Bundle Temperatures

The pyrometer-measured temperatures on the central rod, a side rod, and the shroud are shown in Figure 2. The center rod shows the most pronounced peak, reaching a maximum temperature of about 2250°C. The center rod probably had the smallest net radial heat losses, due to radiative contributions from the surrounding rods and higher local steam temperatures, and the temperature therefore escalated first. The rapid temperature turnaround of the center rod was probably due to molten zircaloy runoff from the reaction zone. The temperature of the side rod did not rise nearly as rapidly. The observed temperature rise was due primarily to the input electric power.

The greater heat losses to the surroundings reduced the reaction rate and prevented a marked temperature escalation from occurring.

A temperature drop from 58 to 60 minutes was detected by all three pyrometers. Although it is not possible to determine the exact sequence of events for this experiment, it seems plausible that the temperature drop was associated with some form of material movement. From 60 to 65 minutes all three pyrometer measured temperatures increased despite a constant input electric power. Thermocouple temperature measurements 25 mm from the bundle upper end, and 50 mm from the bundle lower end, showed a temperature increase at the upper end and decrease at the lower end during this time period. Presumably the axial electric power distribution changed as a result of melt relocating in the lower part of the bundle.

### 3.2 Posttest Appearance

The bundle insulation and shroud were intact following the test. However, both had become severely embrittled and broke into small pieces during dismantling. The posttest appearance of the bundle after removing the insulation and shroud is shown in Figure 3. The cladding from all nine rods had melted over the center portion of the bundle, liquefied some fuel, flowed down the rods, and frozen in a solid mass near the bottom of the bundle that substantially blocked the coolant flow channels. The shroud adhered to the refrozen mass and could not be completely removed. Near the steam inlet the zircaloy cladding appeared metallic. Near the bottom of the blockage ( 5 cm above the steam inlet) the cladding was significantly oxidized. The cladding at the upper end of the bundle remained intact but was substantially oxidized.

As shown in Figures 4 and 5, oxide spalling and refrozen drops of molten material are evident below the bundle blockage. The refrozen melt shows poor wetting of the solid surfaces as indicated by the large wetting

angles and small contact areas. Several factors influenced the refreezing behavior in this region, including the viscosity and oxygen content of the melt, and the relatively cold fuel rod surfaces.

Within the bundle blockage (Figure 4), the refrozen melt has a smooth surface and wet the remaining fuel rod sections rather well (small wetting angles and large contact surfaces). The melt had obviously interacted with the oxidized fuel rods and with steam. A large amount of powdery rubble, primarily fuel that probably fractured during cooldown, was found on top of the blockage.

### 3.3 Posttest Examination

#### 3.3.1 Appearance of the Bundle Blockage

After visual and photographic examination, the bundle was encapsulated in epoxy for metallographic, electron microprobe (EMP), and scanning electron microscope (SEM) examinations, and sectioned as shown in Figure 5. Figures 6 and 7 show photographs of the cross sections through the blocked region at 116, 106, 96 and 86 mm above the bottom of the bundle. The cross sections are shown approximately 3 times actual size.

The cross sections at 116 and 106 mm above the bottom of the bundle (Figure 6) clearly show that the bundle was almost completely blocked by refrozen melt, leaving only a small hole for steam flow between the four rods on the upper right. Considerable steam oxidation is evident along the edges of the hole. In contrast, the hole that first appears in Figure 6 at 106 mm between the lower three rods and the shroud shows less oxidation. Stagnant steam was trapped in this region and the oxidation was therefore limited.

In Figure 6 the oxidized cladding appears to have been dissolved by molten material at many locations. Faint outlines show the locations of the original cladding boundaries. The UO<sub>2</sub> ring pellets are only partially dissolved. The remains of oxidized cladding are visible in the upper left region of the cross section at 106 mm.

Figure 7 shows that the steam-melt-fuel rod interaction history varied in different regions of the same cross section. At 96 mm the melt between the four rods on the upper left has not appreciably interacted with the oxidized cladding, in contrast to the melt in the lower regions of the photographs. The melt in the upper left may have: (a) arrived at a different time, (b) had a different temperature, (c) had a different composition, or (d) some combination of all three.

The extent to which the cladding oxidized prior to melt contact, and the extent of dissolution of the oxide by the melt, can be quite different. The center rod at 96 mm illustrates four distinct cladding regions, beginning clockwise from the lower right: (a) strong cladding/melt interaction such that the two are visually indistinguishable, (b) weaker cladding/melt interaction, with the interface still visible, (c) oxidized cladding/melt contact with very little interaction, and (d) severely oxidized cladding with no melt contact.

The objectives of the posttest examination of the bundle, as suggested by the blockage appearance, were to investigate: (a) dissolution of  $UO_2$  by the melt, (b) the formation of typical phases in the melt, (c) the dissolution of  $ZrO_2$  by the melt, and (d) the oxidation of the melt by steam.

### 3.3.2 Dissolution of $UO_2$ by the Melt

When the cladding reaches the melting point of zircaloy, the unoxidized cladding melts. Liquid zircaloy in contact with  $UO_2$  dissolves  $UO_2$ . The dissolution of  $UO_2$  by molten zircaloy has been extensively investigated /5, 6/. Figure 8 illustrates this interaction for our test in a high magnification SEM photograph at 106 mm. Along the interface between the melt and the  $UO_2$  pellet (on the right) are thin regions rich in uranium, which resulted from the reduction of the  $UO_2$  by the melt. Particles of  $UO_2$  broke away from the pellet which quickened the dissolution. At test temperatures the melt was a uniform mixture of U, Zr and O (one or two-phase, depending on the oxygen content) which decomposed into three phases on cooling /5, 6/.

### 3.3.3 Phases in the Refrozen Melt

Three distinct phases were found in the refrozen melt, two metallic and one ceramic: (a) oxygen-stabilized  $\alpha$ -Zr(O) containing some U, (b) a uranium-rich (U,Zr) alloy, and (c) ceramic  $UO_2$  containing some Zr. Figure 9 shows the results of microprobe analyses of the melt at the same relative location in three cross sections at different axial elevations. The locations were chosen where the melt had not been in direct contact with either a fuel rod simulator or steam. The compositions of each phase are shown in atom percent, and it is clear that the number of phases and phase compositions do not vary with axial location. The grain sizes do vary, increasing with increasing elevation. Presumably the melt remained hot longer at the higher elevations due to its greater mass, and the larger grains formed during the slower cooldown.

Visual comparison of Figure 9 with homogeneous  $UO_2/Zr$  melt standards indicates that the melt contains roughly 40 wt.%  $UO_2$  /6/. Assuming all of the zircaloy cladding in a given axial section melted and dissolved fuel, 40 wt.%  $UO_2$  in the melt corresponds to a reduction of the original  $UO_2$  pellet radius from 4.6 to about 4.2 mm. At the higher elevations (Figure 6) the  $UO_2$  ring pellets are smaller by approximately this amount. At the lower elevations (Figure 7), substantial thinning of the ring pellets is not evident.

### 3.3.4 Dissolution of Oxidized Cladding by the Melt

The extent of dissolution of oxidized cladding varied substantially throughout the blockage, both axially and radially (Figures 6 and 7), indicating that portions of the melt flowed down and refroze at different times. At 106 mm (Figure 6) a section of oxidized cladding from the left side rod was in contact with melt on both the inside and outside surfaces. This section of cladding, surrounded by melt, is shown at higher magnification in an SEM photograph in Figure 10 with EMP analysis results.

A thin strip of  $ZrO_2$  is evident in the middle of the oxidized cladding region, bordered on both sides by  $\alpha$ -Zr(O). Most likely, the strip of

cladding was originally completely  $ZrO_2$ , which was then chemically reduced by the melt to  $\alpha-Zr(O)$ . The cladding section contains no uranium. The melt on either side of the cladding section contains two phases. The composition of the light gray Zr-rich metallic phase (points 1,3, and 11 in Figure 10) corresponds roughly to that of  $\alpha-Zr(O)$  with a small amount of uranium. The dark gray ceramic phase (points 2 and 10) is a  $(U,Zr)O_2$  solid solution. No  $(U,Zr)$  metallic phase was found.

The overall oxygen content of the melt (Figure 10) is higher than that found in regions of the melt discussed earlier, which is in agreement with the phase diagram. At lower oxygen contents, two metallic phases ( $\alpha-Zr(O)$  and a  $(U,Zr)$  alloy) are in equilibrium with  $UO_2$ . At higher oxygen contents, one metallic phase ( $\alpha-Zr(O)$ ) is in equilibrium with two ceramic phases ( $UO_2$  and  $ZrO_2$ ), and no  $(U,Zr)$  is present. Under non-equilibrium conditions a single  $(U,Zr)O_2$  phase is present at room temperature rather than  $UO_2$  and  $ZrO_2$ .

### 3.3.5 Oxidation of Cladding and Melt by Steam

A single hole existed in the blockage (Figures 6 and 7). The hole boundary was severely oxidized by flowing steam. Figure 11 shows a high magnification SEM photograph with microprobe results of the hole boundary (location 4 of the cross section at 106 mm). From left to right, the figure shows  $UO_2$  pellet, "refrozen melt", "oxidized melt", and  $ZrO_2$ . The "oxidized melt" is a homogeneous  $(U,Zr)O_2$  mixed oxide. This melt possibly refroze at a relatively high temperature as a result of increased oxygen content due to oxygen diffusion through the  $ZrO_2$ . The "refrozen melt" appears to have a fine two phase lamellar microstructure, although the microprobe results did not resolve this. The lower overall uranium content suggests a mixture of  $\alpha-Zr(O)$  and  $(U,Zr)O_2$ . This melt probably froze during cooldown.

#### 4. Summary

The center rod of the nine rod bundle escalated to a maximum temperature of 2250°C. Runoff of the melt apparently limited the escalation. Posttest visual examination of the bundle showed that cladding from every rod had melted, liquefied some fuel, flowed down the rod, and frozen in a solid mass that substantially blocked all flow channels. A large amount of powdery rubble, probably fuel that fractured during cooldown, was found on top of the blockage.

Metallographic, EMP, and SEM examinations showed that the melt had dissolved both fuel and oxidized cladding, and had itself been oxidized by steam. Depending on the overall oxygen content, the melt at room temperature contained: (a) three phases (low oxygen content),  $\alpha$ -Zr(O), a uranium-rich (U,Zr) alloy, and (U,Zr)O<sub>2</sub>, or (b) two phases (high oxygen content),  $\alpha$ -Zr(O) and (U,Zr)O<sub>2</sub>. The higher oxygen content indicates dissolution of ZrO<sub>2</sub> as well as UO<sub>2</sub>. The melt contained roughly 40 wt.% UO<sub>2</sub>. Where the local oxidation was very severe, such as in steam contact, only the (U,Zr)O<sub>2</sub> phase was found in regions presumed to have been molten.

#### 5. Acknowledgment

Thanks are due to D.K. Kerwin-Peck for the thorough critical review, and H. Malauschek and K.P. Wallenfels for the performance of the tests.

## 6. References

1. S. Hagen, S.O. Peck, Temperature Escalation in PWR Fuel Rod Bundles due to the Zircaloy/Steam Reaction: Bundle Test ESBU-1, Test Result Report, KfK-Report 3508, 1983 (in preparation).
2. S. Hagen, "Out-of-pile Experiments on the High Temperature Behavior of Zry 4 Clad Fuel Rods," 6<sup>th</sup> Int. Conf. on Zirconium in the Nuclear Industry, Vancouver, British Columbia, Canada, 28 June - 1 July 1982.
3. S. Hagen, S.O. Peck, Temperature Escalation in PWR Fuel Rod Simulators due to the Zircaloy/Steam Reaction: Tests ESSI 1-3, Test Results Report, KfK-Report 3507, 1983 (in preparation).
4. S. Hagen, S.O. Peck, Temperature Escalation in PWR Fuel Rod Simulators due to the Zircaloy/Steam Reaction: Tests ESSI 4-11, Test Results Report, KfK-Report 3557, 1983 (in preparation).
5. P. Hofmann, D.K. Kerwin-Peck, P. Nikolopoulos, "Physical and Chemical Phenomena associated with the Dissolution of Solid UO<sub>2</sub> by Molten Zircaloy-4", 6<sup>th</sup> Int. Conf. on Zirconium in the Nuclear Industry, Vancouver, British Columbia, Canada, 28 June - 1 July, 1982.
6. P. Hofmann, D.K. Kerwin-Peck, "Chemical Interaction of Zircaloy-4 with UO<sub>2</sub> above 1700°C under Nonoxidizing Conditions," paper to be presented at the Int. Meeting on LWR Severe Accident Evaluation, Cambridge, Massachusetts, August 28 - September 1, 1983.

## 7. List of Figures

- Fig. 1: ESBU-1 Axial and Radial Cross sections and the Locations of the two-color Pyrometers.
- Fig. 2: Temperatures on the Central Rod (Z). Side Rod (N) and Shroud (S) 145 mm from the Upper End of Cladding Compared to the Electric Power input for ESBU-1.
- Fig. 3: 3x3 Bundle of ESBU-1 after Removal of the Upper Part of the Shroud.
- Fig. 4: Enlargement of the Blocked Region of ESBU-1 Illustrating the Wetting Behavior of the Melt.
- Fig. 5: Schematic Diagram Showing Axial Elevations of the ESBU-1 Cross Section.
- Fig. 6: Cross Sections of ESBU-1 at 116 and 106 mm above the Bottom of the Bundle.
- Fig. 7: Cross Sections of ESBU-1 at 96 and 86 mm above the Bottom of the Bundle.
- Fig. 8: Dissolution of  $UO_2$  by the Melt.
- Fig. 9: Microprobe Analysis of the 3 Phases in the Refrozen Melt.
- Fig. 10: Microprobe Analysis of Remaining oxidized Cladding in Contact with Refrozen Melt.
- Fig. 11: Oxidation of Cladding in Continuous Steam Flow.

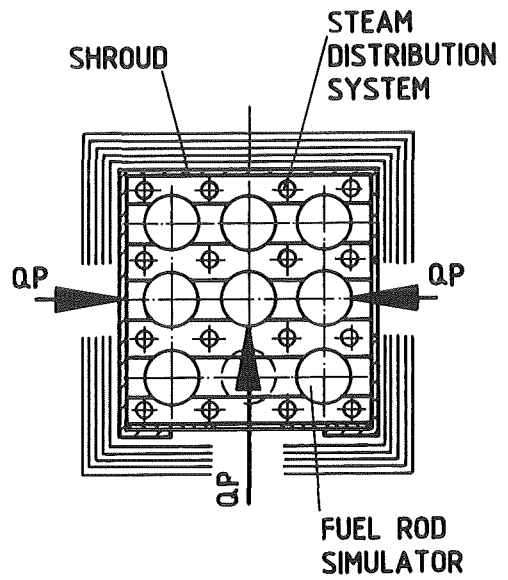
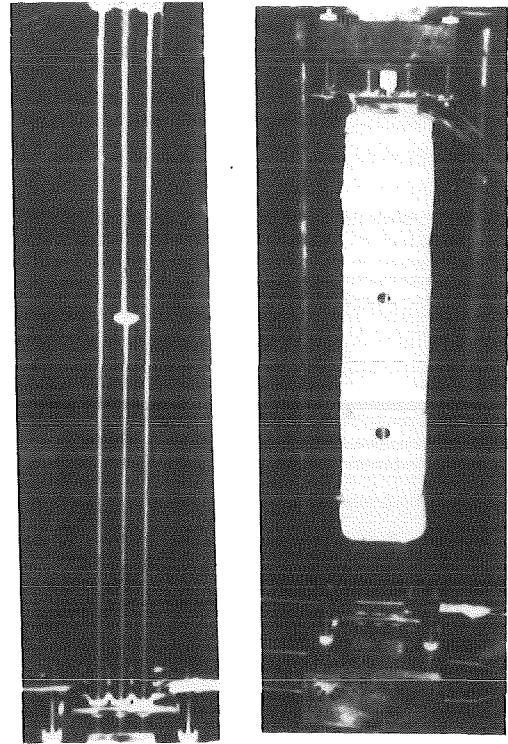
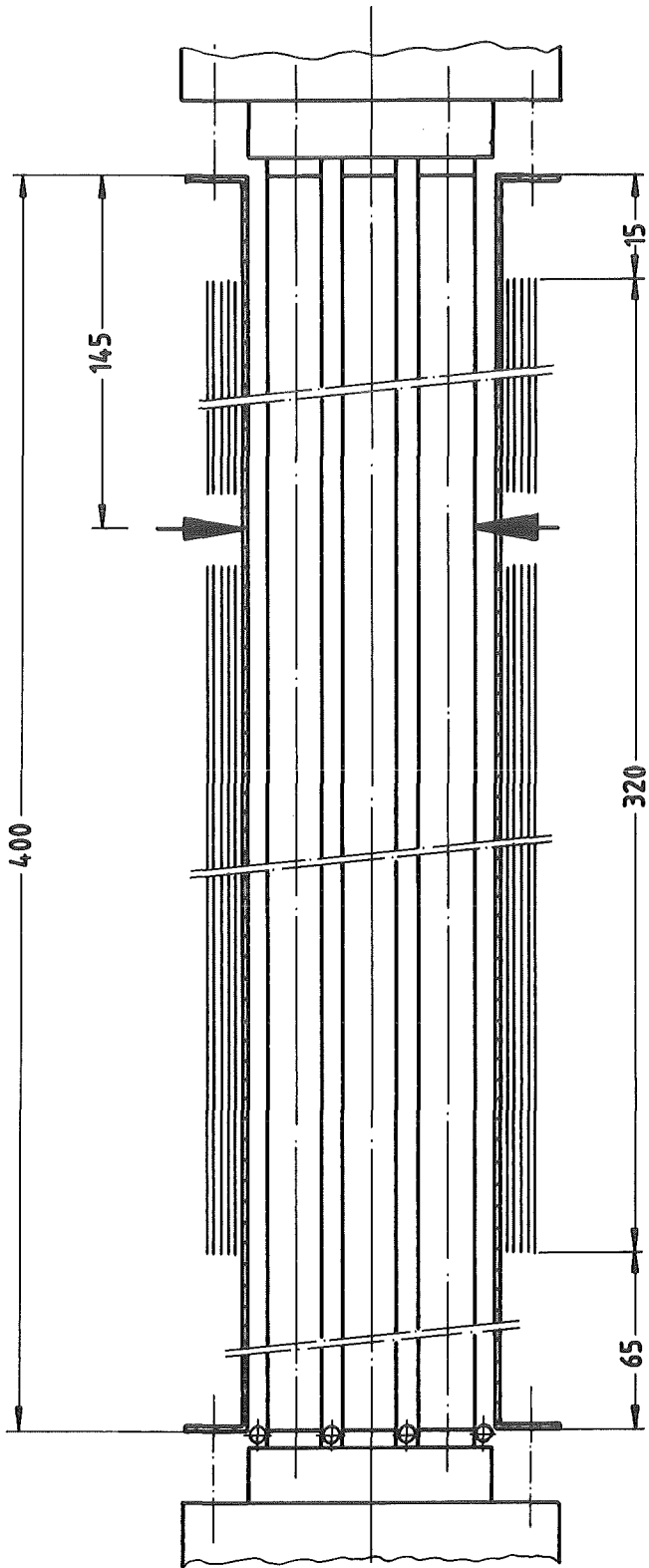
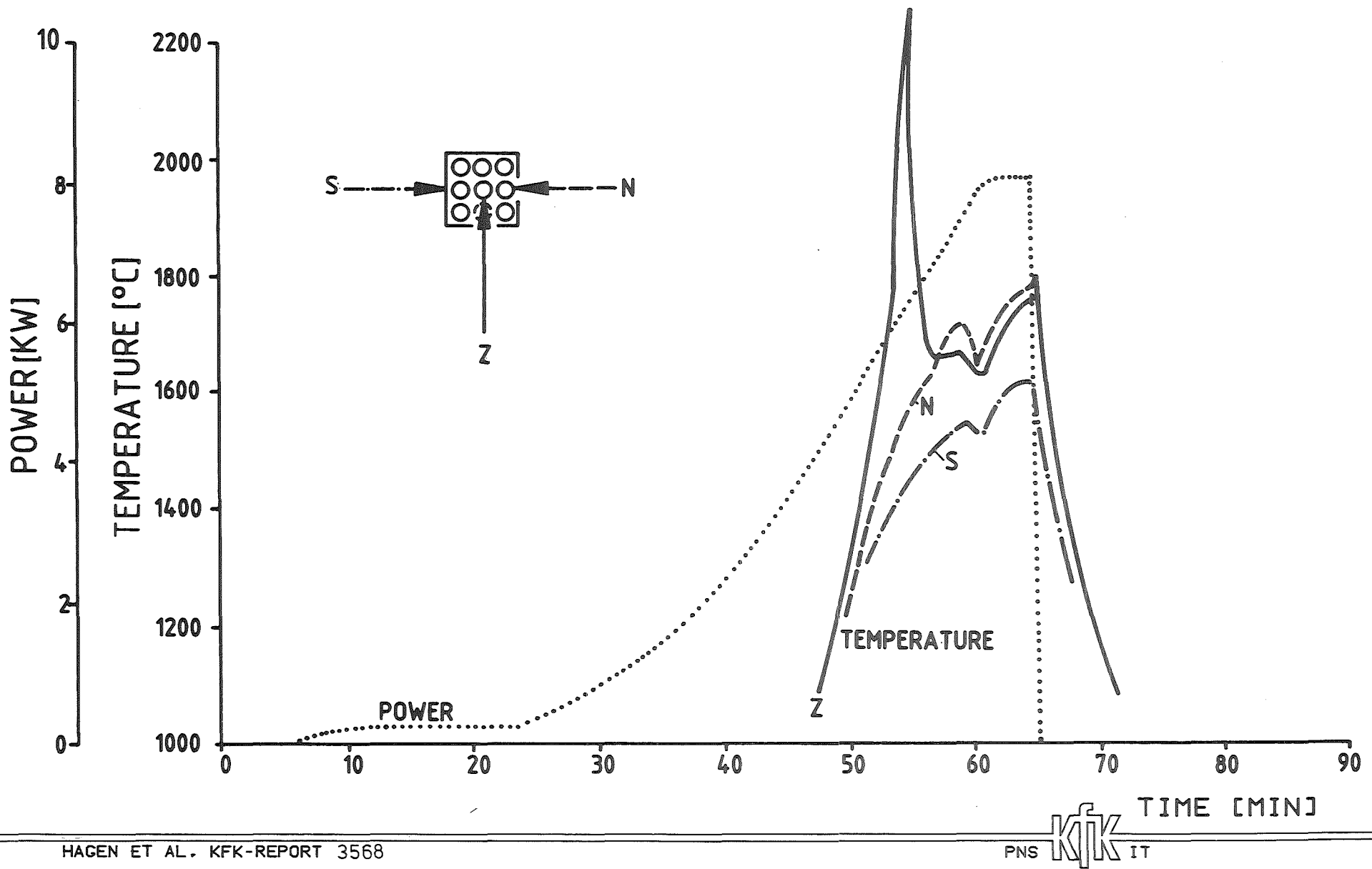


FIGURE 1: ESBU-1 AXIAL AND RADIAL CROSS SECTIONS AND THE LOCATIONS OF THE TWO-COLOR PYROMETERS



HAGEN ET AL., KFK-REPORT 3568

PNS **KIK** IT

FIG.2 : TEMPERATURES ON THE CENTRAL ROD (Z), SIDE ROD (N) AND SHROUD (S) 145 MM FROM THE UPPER END OF CLADDING COMPARED TO THE ELECTRIC POWER INPUT FOR ESBU-1

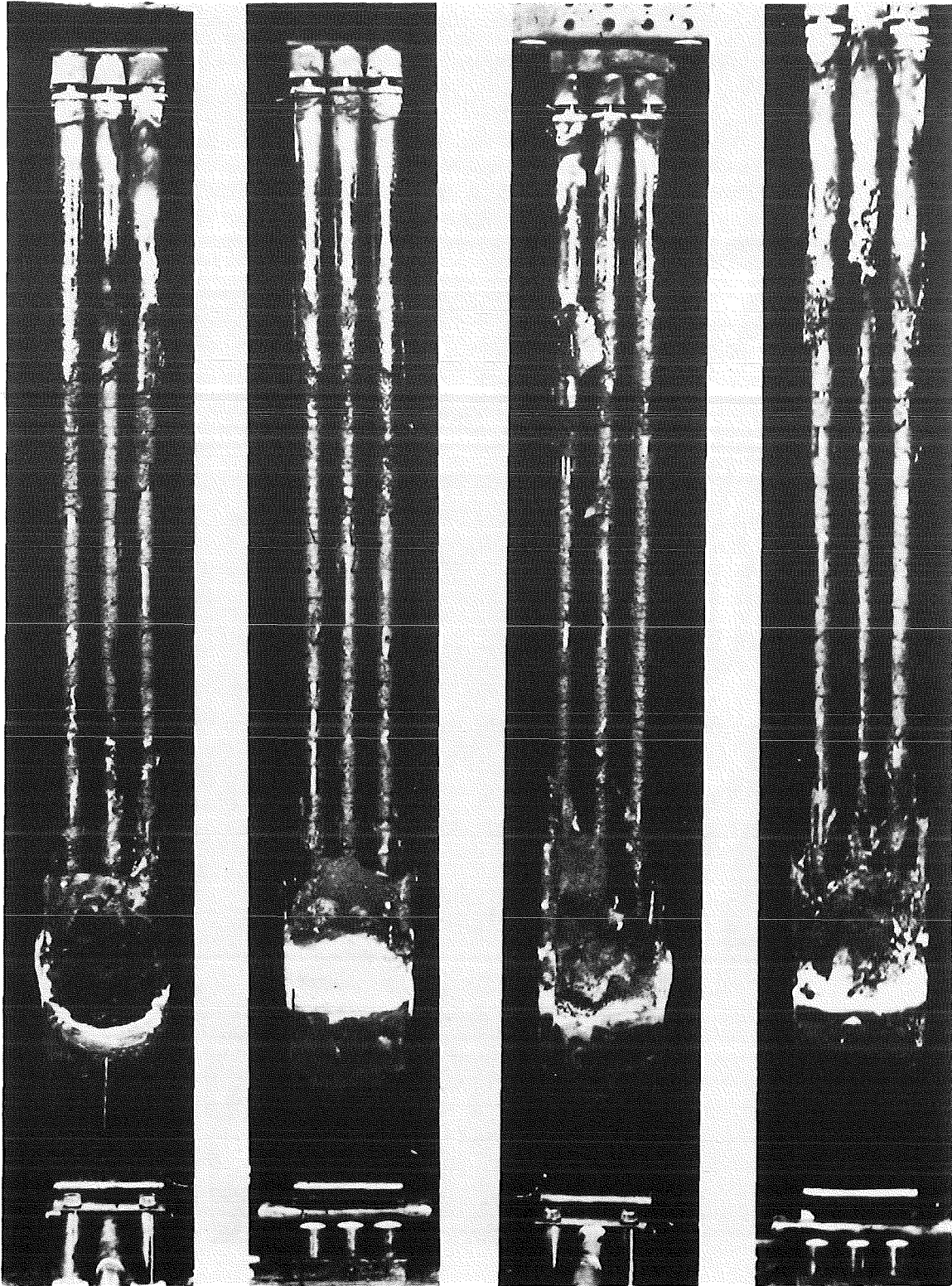


FIGURE 3: 3x3 BUNDLE OF ESBU-1 AFTER REMOVAL OF THE UPPER PART OF THE SHROUD

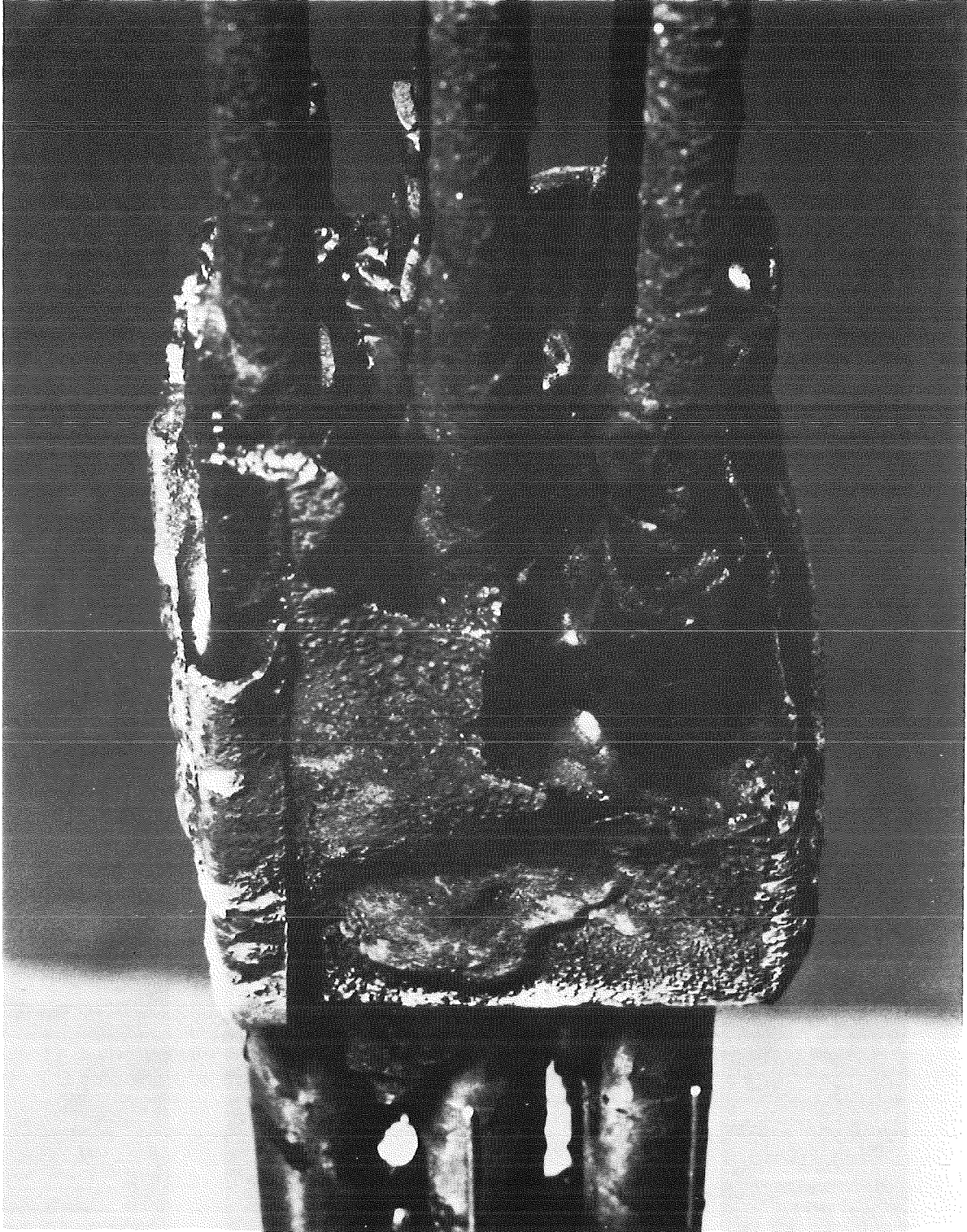


FIGURE 4 : ENLARGEMENT OF THE BLOCKED REGION OF ESBU-1  
ILLUSTRATING THE WETTING BEHAVIOR OF THE MELT

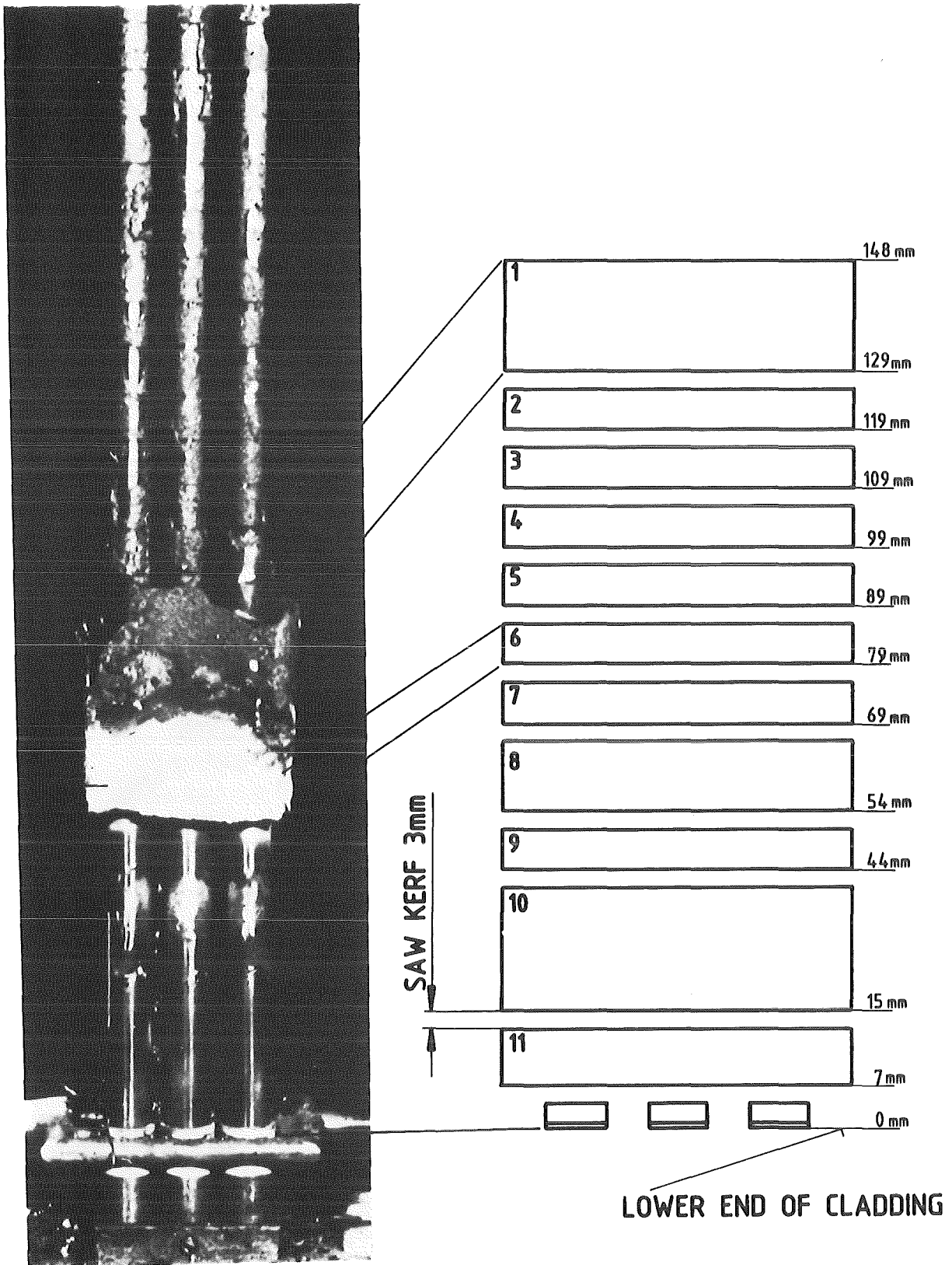
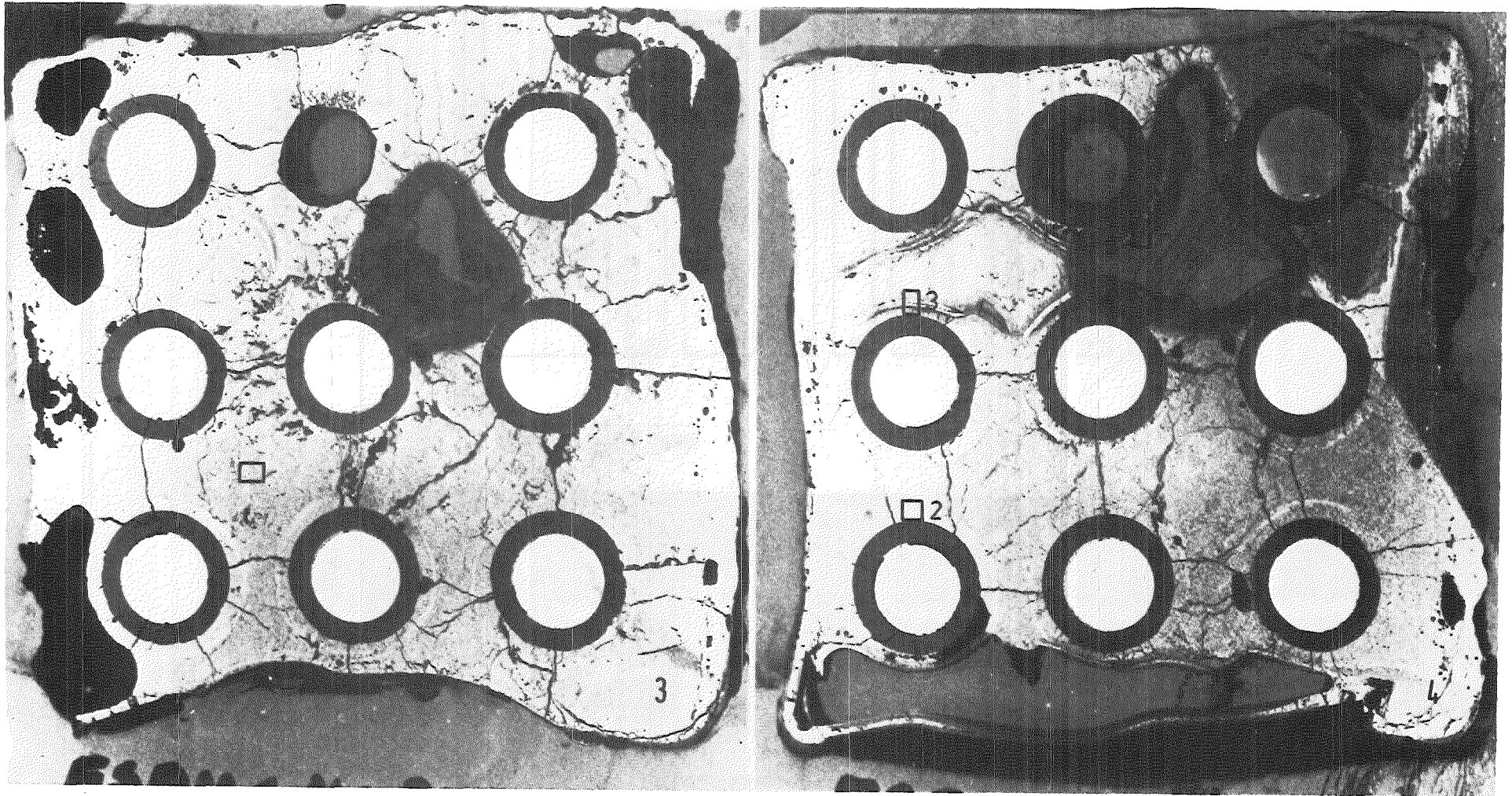


FIGURE 5: SCHEMATIC DIAGRAM SHOWING AXIAL ELEVATIONS OF THE ESBU-1 CROSS SECTIONS.

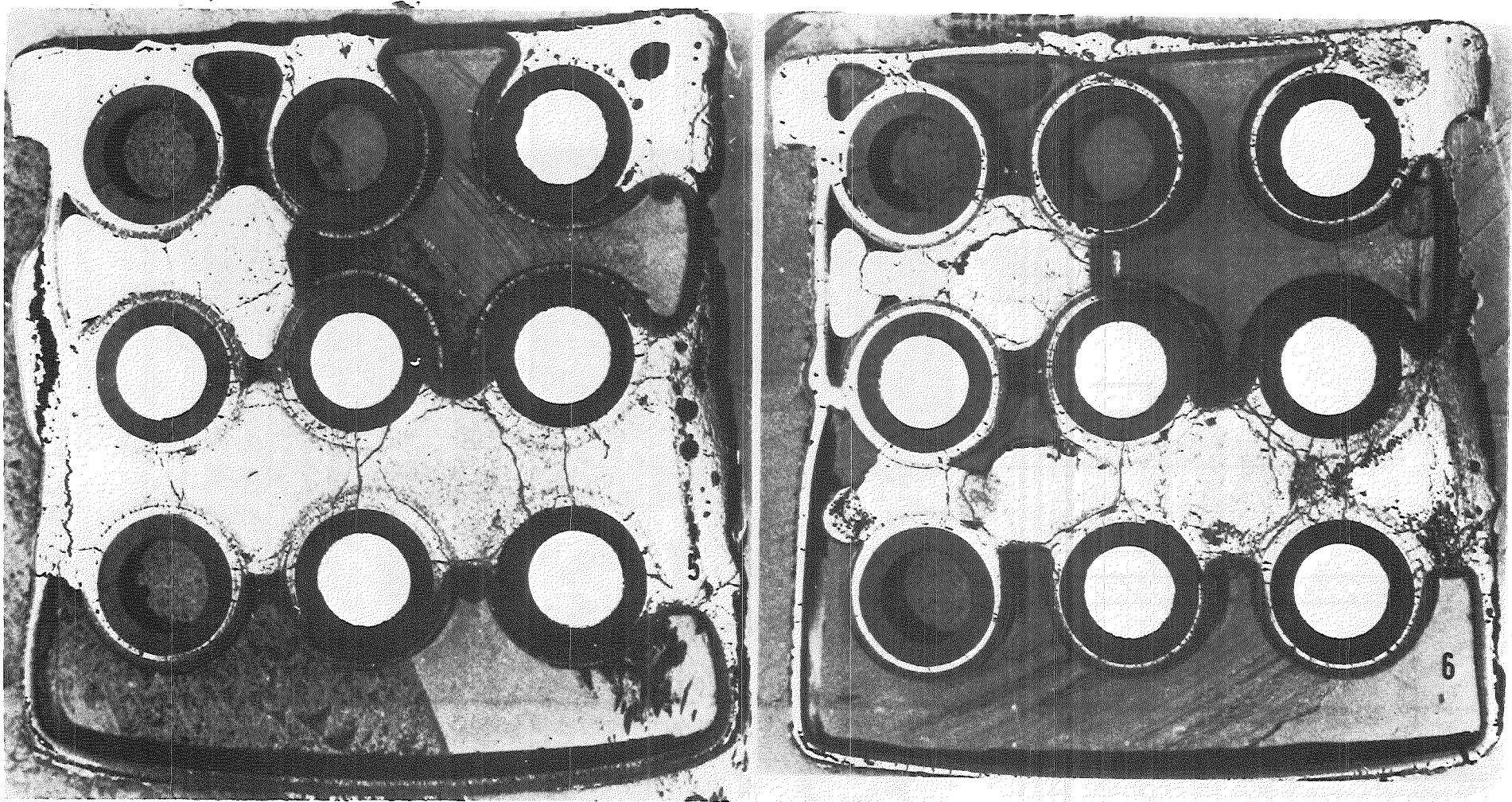
116 mm

106 mm



- 18 -

FIGURE 6: CROSS SECTIONS OF ESBU-1 AT 116 AND 106 MM ABOVE THE BOTTOM OF THE BUNDLE



96 mm

86 mm

HAGEN ET AL. KFK-REPORT 3568

PNS **kfk** IT

FIGURE 7: CROSS SECTIONS OF ESBU-1 AT 96 AND 86 MM ABOVE THE BOTTOM OF THE BUNDLE

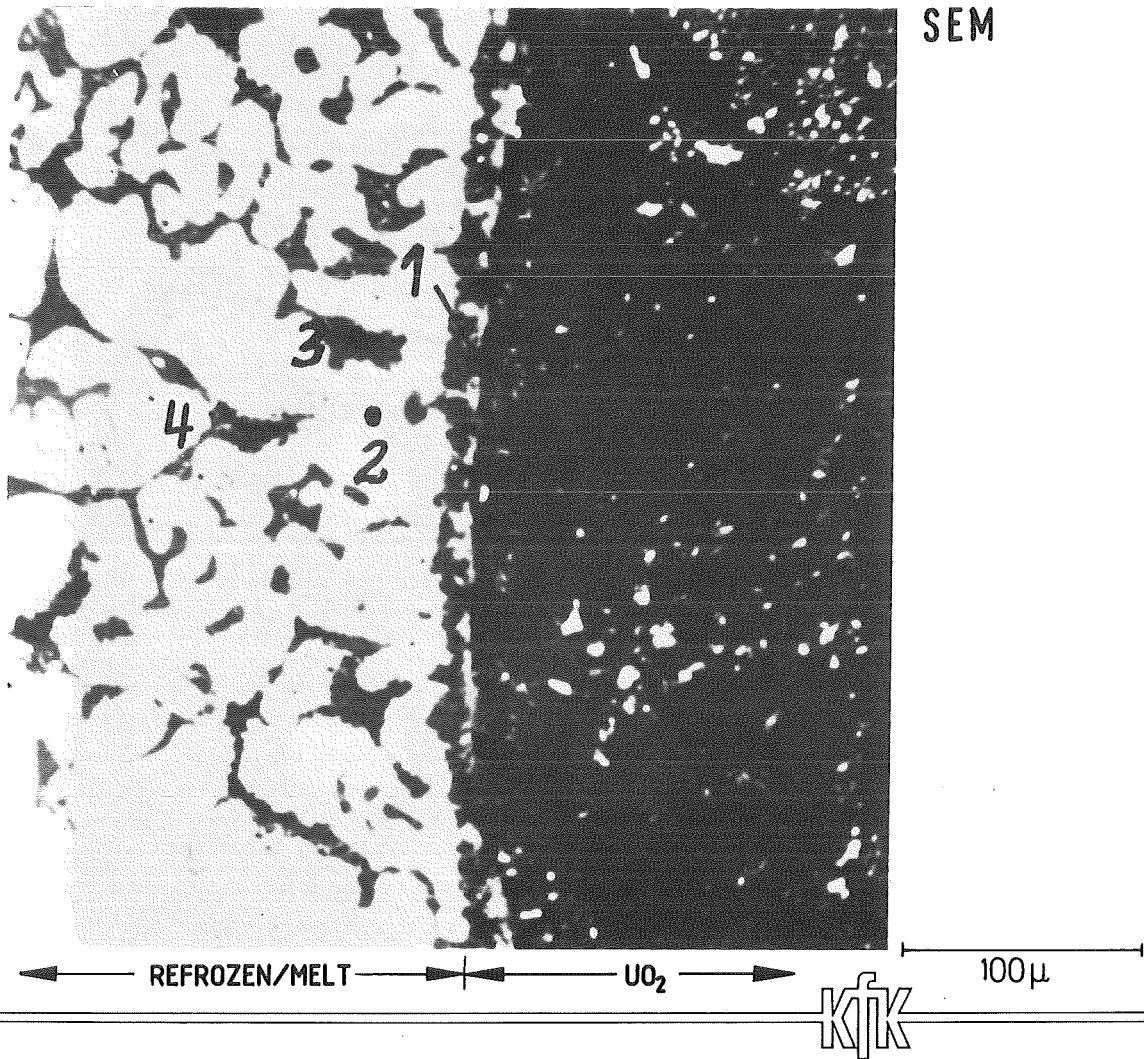
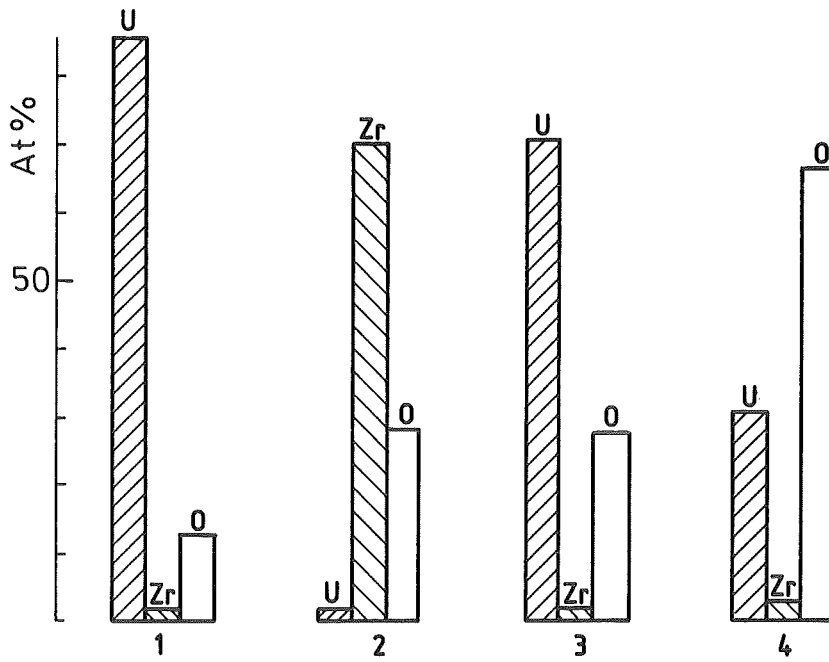
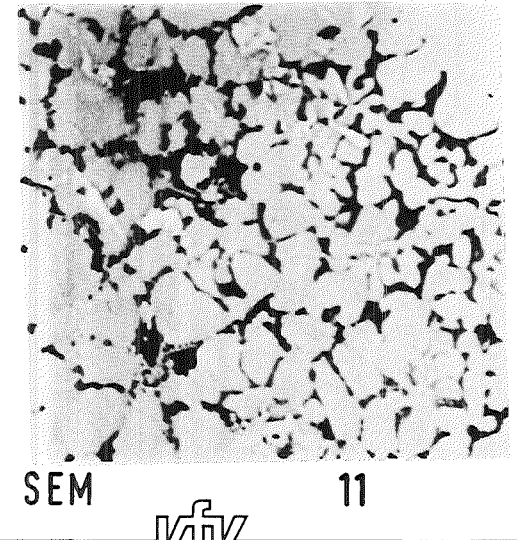
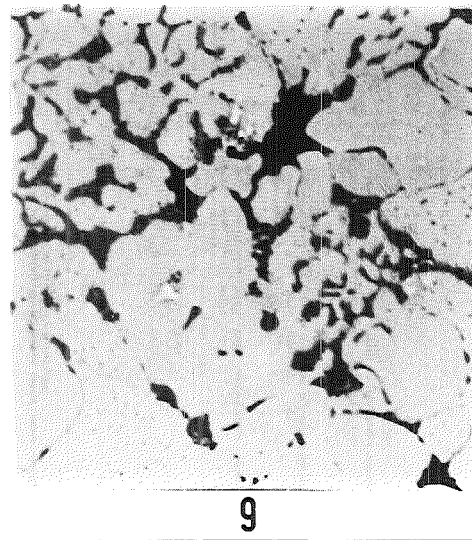
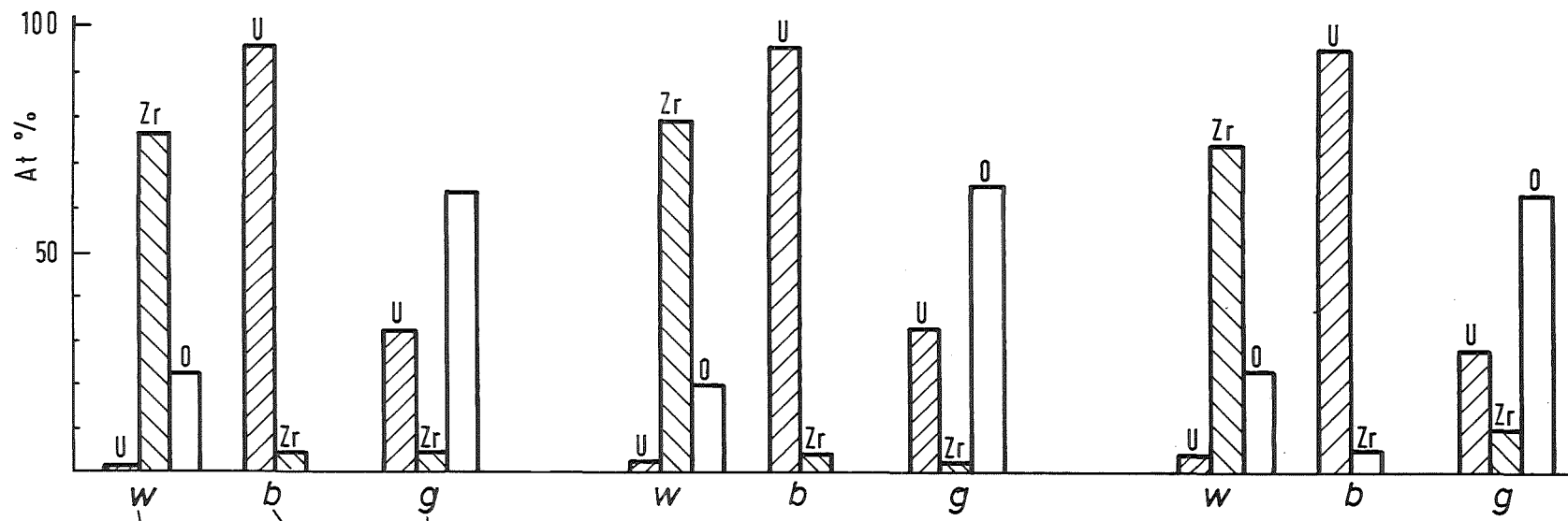


Fig. 8:  
DISSOLUTION OF UO<sub>2</sub> BY THE MELT  
ESBU-1: LOCATION 2 OF CROSS SECTION 4 (106mm), UNCORRECTED O-VALUES



PNS KJK IT

FIG. 9: MICROPROBE ANALYSIS OF THE 3 PHASES IN THE REFROZEN MELT  
 ESBU-1: CROSS SECTIONS 3 (116 MM), 9 (51 MM) AND 11 (7 MM ABOVE BUNDLE); CORRECTED O-VALUES

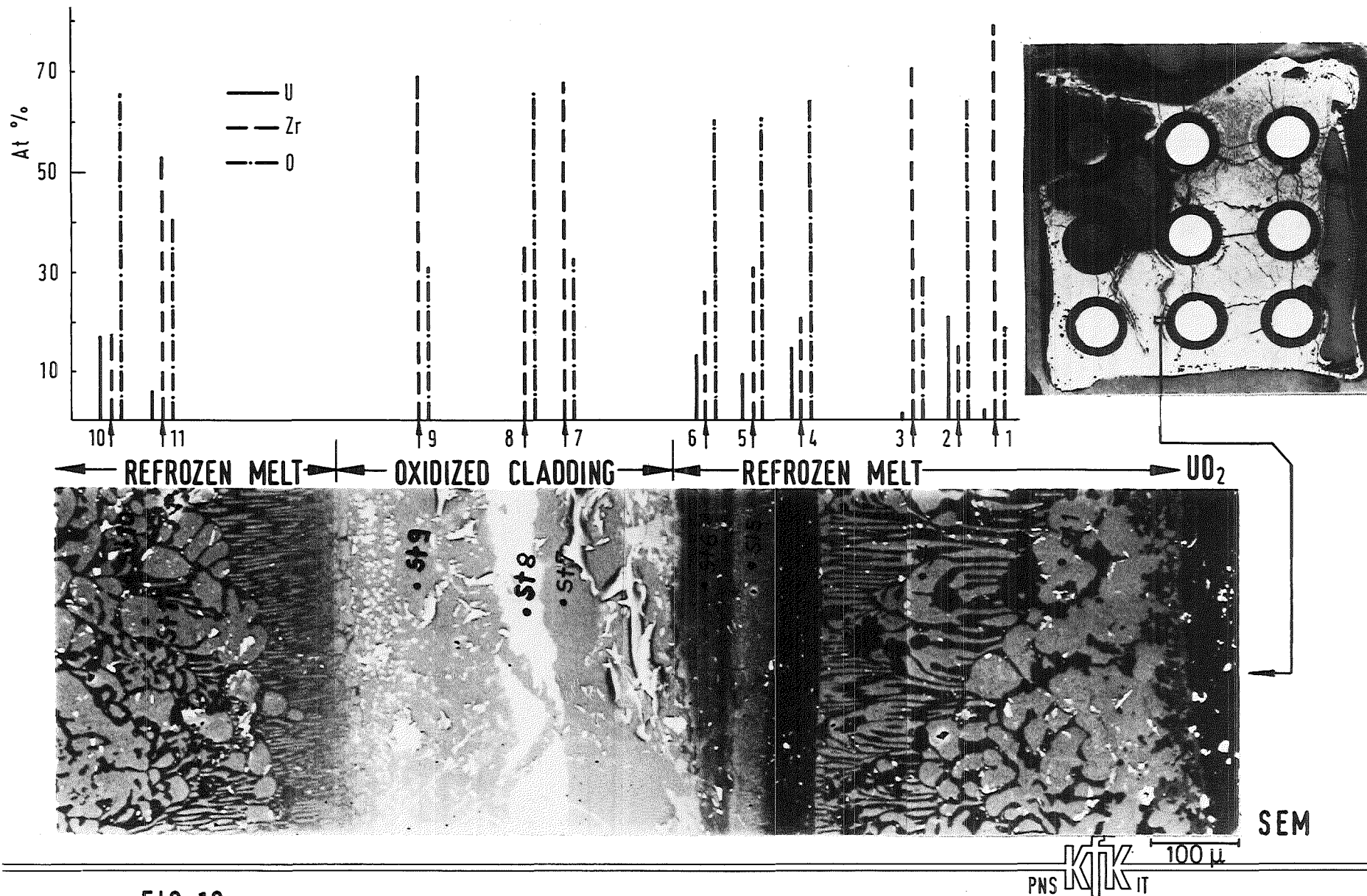


FIG. 10:  
 MICROPROBE ANALYSIS OF REMAINING OXIDIZED CLADDING IN CONTACT WITH REFROZEN MELT  
 ESBU-1: LOCATION 3 OF CROSS SECTION 4 (106 mm ABOVE BOTTOM), UNCORRECTED O-VALUES

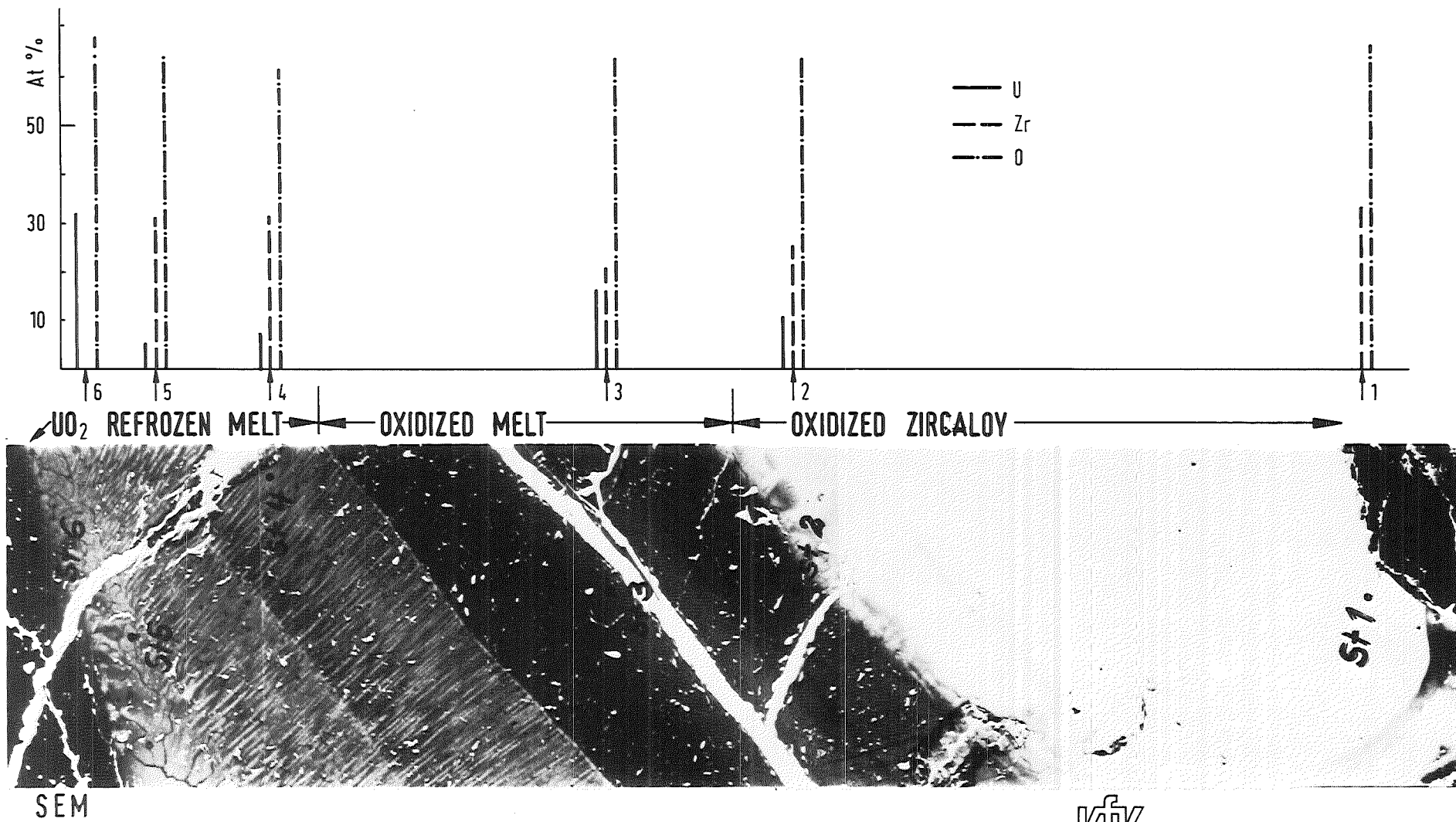


FIG. 11: OXIDATION OF CLADDING IN CONTINUOUS STEAM FLOW  
 ESBU-1: LOCATION 4 OF CROSS SECTION 4 (106mm)